Simovski, Konstantin; Sharifian Mazraeh Mollaei, Masoud; Voroshilov, Pavel

Fluorescence quenching by plasmonic nanoantennas

Published in:
Physical Review B

DOI:
10.1103/PhysRevB.101.245421

Published: 15/06/2020

Document Version
Publisher's PDF, also known as Version of record

Please cite the original version:
Simovski, K., Sharifian Mazraeh Mollaei, M., & Voroshilov, P. (2020). Fluorescence quenching by plasmonic nanoantennas. *Physical Review B*, *101*(24), Article 245421. https://doi.org/10.1103/PhysRevB.101.245421

Fluorescence quenching by plasmonic nanoantennas

C. R. Simovski,[1,2] M. S. M. Mollaei,[1] and P. M. Voroshilov[2]
[1]*Department of Electronics and Nanoengineering, Aalto University, P.O. Box 15500, FI-00076 Aalto, Finland*
[2]*University ITMO, Kronverkski 47, 197101, St. Petersburg, Russia*

(Received 8 April 2020; revised manuscript received 1 June 2020; accepted 2 June 2020; published 15 June 2020)

Generalizing a previously developed analytical model of metal-enhanced fluorescence to the case of the strong coupling between a quantum emitter and a plasmonic nanoantenna, we study the fluorescence quenching in the strong coupling regime. When the nanoantenna is a simple Ag sphere and the quantum emitter approaches to its surface the fluorescence turns suppressed (both dipole and quadrupole moments of the system vanish) in the whole spectral range. However, if the nanoantenna is a plasmonic dimer with a tiny gap between two plasmonic nanoparticles, and the coupling grows due to the increase of the emitter dipole moment, the fluorescence quenching never occurs. This unexpected result explains why the nanolaser regime can be achieved with these nanoantennas, whereas a simple nanosphere coupled to quantum emitters can be a spaser.

DOI: 10.1103/PhysRevB.101.245421

I. INTRODUCTION

Fluorescence quenching (see, e.g., in Ref. [1]) is an important destructive factor in a powerful technique of optical nanosensing called metal-enhanced fluorescence, sometimes also called plasmon-controlled fluorescence [2–5]. The dynamic fluorescence quenching arises when the near-field coupling between a plasmonic nanoantenna (PNA) and quantum emitters (QEs) exceeds a certain critical value [2–7]. Enhancement of the fluorescence of such QEs as organic molecules and quantum dots in the presence of a PNA is referred as the Purcell effect and described by the radiative Purcell factor larger than unity [2,8]. The maximal enhancement is granted when the coupling is sufficient but still rather weak [2,9–11]. A gradual increase of the coupling of a QE and a PNA reshapes the fluorescence spectrum, decreases the radiative Purcell factor compared to its resonant value evaluated for the optimal coupling and, finally, results in a decrease of the fluorescence due to the PNA presence [3,4]. Then the radiative Purcell factor turns smaller than unity in the whole fluorescence spectrum [5,13]. This decrease as a function of the coupling parameter (proportional to the Rabi frequency shift in the regime of the strong coupling) occurs very fast and, therefore, can be considered as a threshold effect [3–5,12,13]. This is the reason why this suppression of fluorescence is called quenching.

This quenching is a prerequisite for generation of a coherent localized surface plasmon in a PNA [14–16]. The system in which the plasmon is generated is called spaser [17–19]. In accordance to [14–16], the spaser regime corresponds not only to a sufficiently high emission level but also to nonradiative transfer of the emitted power into PNA. This is possible if the total polarization of the system is negligibly small and the system does not radiate into ambient. In this linear regime, before the nonlinearity arises in the system, the emitted power accumulates in the PNA in the form a growing plasmon oscillation. Further, in the generation regime, this plasmon is restricted by the nonlinearity and becomes coherent. Simultaneously, a weak, almost isotropic and coherent emission arises and a very narrow emission line substitutes the usual Lorentzian line of the spontaneous fluorescence [17–19]. Spasers form an interesting and practically important [14,19,20] direction of nanophotonics. Therefore it is also important to understand which types of PNAs are suitable for spasers and which types are not.

In 2009, an experimental demonstrator of a spaser was claimed for a primitive PNA performed as a plasmonic nanosphere (PNS) covered with a shell of fluorescent molecules separated a nanometer dielectric gap from the PNS [19]. Here it is worth to notice that one fluorescent molecule cannot grant a spaser – its fluorescence capacity turns saturated when the pumping level grows (a fluorescent QE is basically a two-level system that cannot simultaneously radiate more than one photon). A sufficient amount $N \gg 1$ of fluorescent molecules or quantum dots coupled to a PNS so that their fluorescence quenches together with a sufficiently strong pumping grant the spaser regime. Several examples of spasers have been reported after it [19,20], and in all of them the PNA was a PNS. Some scientists do not recognize these these structures were spasers and attribute the observed effect to amplified spontaneous emission. We do not aim to intervene into this discussion and will simply show that with such a PNA as a simple PNS the suppression of the fluorescence is possible. Meanwhile, no one work is known where the spaser operation would be claimed, at least theoretically, for a good PNA such as a plasmonic bowtie, a plasmonic split-ring resonator or a plasmonic oligomer. Here the term good PNA refers to an antenna with very high radiative Purcell factor ($F_P > 100$) offered to an emitter located at the optimal distance from the metal surface. This also means the very high local intensity enhancement at the same distance (the mathematical identity of these two parameters of a PNA for the unpolarized case was recently proved in Ref. [21]). Next, in all available works about the dynamic fluorescence quenching,

PNAs were similarly poor—simple nanospheres, nanodisks or nanorods which grant a modest local field enhancement (maximal F_P is of the order of 10). So, for good PNAs both the dynamic fluorescence quenching and the spaser operation were, to our knowledge, never claimed. It is reasonable to assume that there is some physics which prohibits the fluorescence quenching for good PNAs and this is the reason why they cannot operate as spasers.

In work [22], a semiclassical theory of a bowtie nanolaser was developed. Let us stress that a nanolaser is not a spaser. It is an analog of a usual laser whose resonator is a nanocavity—nanogap of a bowtie nanoantenna. This was explained in [23] where the possibility of generating the induced emission in a bowtie PNA with quantum emitters in its gap had been predicted prior to Ref. [22]. In the transition regime of a nanolaser, the total polarization of the system grows in time due to the plasmon-stimulated emission. In the steady regime, the induced radiation of the nanolaser is dipole radiation. On the contrary, in the transition regime of a spaser, a near-field mode of the localized surface plasmon grows whereas the radiation is fully suppressed. This is so because the polarization of the plasmon generated in the PNA cancels out with the polarization generated in the QEs. The induced radiation of the spaser in the steady regime is nonzero, as well as that of the nanolaser, but it is much weaker, not directive and refers to a nonlinear regime, whereas the suppression of radiation in a spaser refers to the linear, transient regime. In work [24], the difference between the nanolaser and a spaser is discussed in details. In an experimental implementation of a nanocavity-based laser from work [25] the operation principle is the same as in works [22–24]. Notice, that the regime of a nanolaser demands a higher pumping than the regime of the spaser [24] because the pumping should overcompensate the radiation loss. Perhaps, this is the reason why the nanolaser based on a single bowtie PNA has not been experimentally demonstrated, yet. Meanwhile, nanolasers based on periodic arrays of bow-tie PNAs and split-ring resonators were demonstrated in works [26–28]. These radiating systems generate a coherent light in the regime of the resonant far-field coupling between PNAs. This regime is favorable for generation because such the electromagnetic coupling damps the scattering by individual PNAs. So, differences between a spaser and a nanolaser are major, and we think, that the name of a lasing spaser employed in Ref. [27] for nanolasers is very misleading. Sooner, they refer to a class of photonic-crystal lasers [29].

In this paper, we present a possible explanation why a good, efficient PNA cannot grant a spaser operation, whereas a simple PNS or, generally speaking, a poor PNA can grant it. We show on a very simple model that the dynamic fluorescence quenching does not occur for a good PNA (a plasmonic dimer in our example), whereas for a simple PNS, it occurs when the coupling exceeds a certain threshold. Thus, the common belief that the fluorescence quenching occurs for all PNA configurations is, in accordance to our model, not correct. Briefly speaking, the fluorescence may quench only if the surface plasmon is excited in a broad band, whereas a good PNA is narrow-band. The details will be clarified below. Thus the necessary condition of a spaser can be fulfilled only for a poor PNA. It worth noticing here, in the available literature one may meet different terms for the dynamic fluorescence quenching [1,3–5,12]—nonradiative Rabi oscillations [15,16,18], nonradiative decay [7,13], nonradiative energy transfer [30], and even Förster resonant energy transfer (FRET) [31]. This variety only reflects a terminological mess, it does not mean different physical mechanisms.

II. DIPOLE MODEL OF PLASMON-CONTROLLED FLUORESCENCE

In 1948, T. Förster has considered the dipole interaction of two molecules. One of them was a two-level QE, another was a multilevel quantum system in which one of upper excited states coincided with that of the first molecule. He has shown that the strong dipole interaction when these molecules are very close to one another results in the nonradiative decay of the emitting molecule because the energy of the photon turns out to be fully transferred to the second molecule where it dissipates due to relaxation. In this regime, the total dipole moment of the molecular dimer vanishes since the dipole moments of two molecules cancel out. Later, this idea was confirmed by quantum calculations and applied to the case when the second molecule was replaced by a PNA (see, e.g., Refs. [30,31]). In the initial model [32], the frequency dispersion of the emitter dipole moment ($d_1(\omega)$ in our notations) keeps unchanged when the gap between tow molecules reduces. In this simplistic approximation, the FRET (NRET) regime is identical to resonant wireless power transfer rediscovered for radio frequencies in work [33]. Though semiclassical models [3–5,12] take the spectral reshaping into account, still classical models of the fluorescence quenching (see in Refs. [6,7]) keeps the same $d_1(\omega)$ when the QE approaches to the PNS. Though the fluorescence quenching occurs for a PNS in this simplistic model as well as it occurs in the accurate semiclassical models and in the experiment, for other plasmonic structures the applicability of this model is not evident. In fact, the reshaping of the fluorescence spectrum and the suppression of the system polarization both hold when the coupling between the QE and the PNA grows. These two processes are evidently competing. The dipole moment suppression is not uniform over the whole fluorescence spectrum. When the optical transition frequency ω_0 and the plasmon resonance frequency coincide, this suppression is maximal (complete) at ω_0 but at the edges of the plasmon resonance it is not complete. And the spectral line not simply reshapes in the strong coupling regime—it experiences the Rabi splitting and two local maxima of fluorescence move apart from other another [15,16,18]). Thus, hypothetically, a situation is possible when one of the frequencies of Rabi oscillations, or both of them, turns outside the band in which the FRET regime may hold. To take this hypothetical situation into account, we either should use an accurate semiclassical approach or, alternatively may use a simple classical approach that would take the spectral reshaping into account. We prefer the second way as simpler and more illustrative.

Such the classical model was suggested in work [34]. The dipole-dipole interaction in this model is based on two basic parameters—electromagnetic interaction coefficient $\overline{\overline{A}}_{12}$ (in the general case dyadic) and dyadic polarizability $\overline{\overline{\alpha}}_2$ of the PNA. The polarizability relates its dipole moment $\mathbf{d}_2$ to the

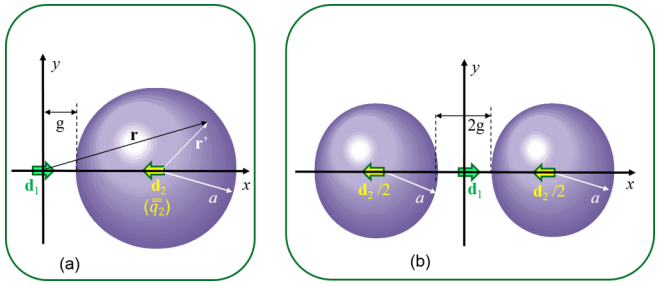

FIG. 1. Two structures under study: (a) QE 1 interacts with PNS 2 being polarized normally to it and (b) QE 1 interacts with plasmonic dimer 2 centering its nanogap.

local field $\mathbf{E}_{12}$ created by the QE at the effective center of the PNA. This coefficient may take into account the nonuniformity of the local field created by QE 1 in the area of PNA 2. The field nonuniformity can be taken into account by the displacement of the effective center of the PNA with respect to its geometrical center. Therefore, the point dipole may be applicable for both QE and PNA even for quite small distances between the QE and the metal surface. The most important polarization case—when the polarization corresponds to the strongest coupling of QE 1 with PNA 2—is the case when the polarization of the QE is collinear with that of the PNA. Figure 1(a) corresponds to a simplest PNA performed as a PNS (Ag or Au nanosphere), panel (b) corresponds to a PNA performed as a dimer of PNSs. For both geometries the strongest coupling arises when the emitter is polarized along x. Then the azimuthal symmetry yields tensors $\overline{\overline{A}}_{12}$ and $\overline{\overline{\alpha}}_2$ to scalar values A_{12} and α_2, respectively. The polarizability α_1 of the quantum emitter is, basically, known—its frequency dispersion is Lorentzian and expressed through the optical transition dipole moment d and frequency ω_0 as follows [8]:

$$\alpha_1 = \frac{(2d^2/\hbar\omega_0)}{1-(\omega/\omega_0)^2 + j\omega\gamma_1/\omega_0^2}, \tag{1}$$

where time dependence $\exp(j\omega t)$ is chosen. For practical fluorescent emitters, the dissipative losses are very low and the damping parameter γ_1 can be identified with the radiative loss of the individual QE. This approximation in accordance to [34,35] gives $\gamma_1 = (2d^2/\hbar\omega_0)\omega_0^2 k^2/6\pi$. Here $k = k_0\varepsilon$ is the wave number of the host medium of permittivity ε (for free space assumed in the present paper as the ambient $k = \omega/c$). Dipole moment $d_1^{(0)}$ of the emitter in absence of the PNA is also a Lorentzian function of frequency whose resonance frequency is ω_0 and damping parameter is γ_1 [8], i.e., $d_1^{(0)} = \hbar\omega_0\alpha_1/2d$.

In presence of PNA 2, described as a dipole scatterer, the following solution for the total dipole moment d_t of the system was strictly obtained in Ref. [34] (see also Ref. [36]):

$$d_t = d_1^{(0)}\frac{1+\alpha_2 A_{12}}{1-\alpha_1\alpha_2 A_{12}^2}, \tag{2}$$

where A_{12} represents the x-polarized electric field E_{12} produced by QE 1 at the effective center of PNA 2, divided by the dipole moment d_1 of the QE. Due to the reciprocity of the structure, the same coefficient $A_{21} = A_{12}$ describes the field E_{21} produced by PNA 2 at the center of QE 1 to which d_2 is referred. If the PNA represents a PNS, as in Fig. 1(a), we may use the low-frequency approximation for the dipole near field and write A_{12} in the form

$$A_{12} = (1 + jkR)/2\pi\varepsilon_0\varepsilon R^3, \tag{3}$$

where R is the distance from QE 1 to the effective center of PNS 2. For PNSs (and spherical nanoshells) this simple model was validated in by comparison with the numerical simulations and the experiment for the cases when the when the gap g exceeded 5 nm for PNSs and 3 nm for nanoshells. In these cases the effective center of the spherical PNS turns out to be its geometric center, i.e., $R = a + g$ if the polarization of 1 and 2 is collinear (it is not so for the parallel polarization).

In the case when $a = 20$–50 nm and $g \geqslant 5$ nm the coupling is rather weak for typical fluorophores such as PM 546 or rhodamine 123, whose matrix element d of the optical transition does not exceed 10 D (see, e.g., in Ref. [37]). Here and below complex permittivities $\varepsilon_{\rm PNS}$ of Ag and Au are taken from [38]. As it is clear from (2), the level of coupling depends on the dimensionless product $\alpha_1 A_{12}$. If $|\alpha_1\alpha_2||A_{12}|^2 \ll 1$, the coupling is weak and we have $d_t = d_1^{(0)}(1+\alpha_2 A_{12})$. In accordance to (1) and (3), for $d = 10$ D, $a = 30$ nm and $g = 0.2a = 6$ nm at the frequency ω_0 we obtain $|\alpha_2 A_{12}|^2 \gg 1$ but $|\alpha_1\alpha_2||A_{12}|^2 \ll 1$. This is so for both Ag and Au nanospheres. The enhancement of fluorescence is maximal in this regime. This enhancement is described by the radiative Purcell factor $F_P \equiv P_{\rm rad}/P_0$ (here $P_{\rm rad}$ is power radiated by the system during the emission of one photon and P_0 is that radiated by individual QE 1). It is evident that $F_P(\omega_0) = |d_t(\omega_0)|^2/|d_1^{(0)}(\omega_0)|^2$. Adopting $d = 8.1$ D—that of rhodamine 123—in (1) and decreasing g we may simulate how the system with a PNS of radius $a = 20$ nm and a rhodamine molecule transfers from the regime of the weak coupling to the strong coupling regime. During this gradual decrease of g we may search the effective center of the PNS that in the case of the strong coupling may shift towards the QE from the geometric center of the sphere. Moreover, we may generalize our dipole model, taking into account the quadrupole moment $\overline{\overline{q}}_2$ induced in the PNS (and higher multipoles if it is really needed). Below we report such the study reducing g from $g = 10$ nm up to $g = 2$ nm (further reduction is useless because the tunneling effect arises for g, 1.5–2 nm [39] and disables the model). Using exact numerical calculations we retrieve the model parameters allowing us to simulate the fluorescence quenching.

It worth noticing here that this study has shown nothing qualitatively new. It has confirmed the known results of the simplistic classical studies, accurate quantum modeling and experiemnts. Namely, a simple PNS offers the fluorescence suppression in the whole spectral rage when the gap g decreases sufficiently—in our example it holds when $g < 2.5$ nm.

However, another scenario of the transition from the weak coupling to the strong one is also possible. It corresponds to the gradual increase of d in the structure depicted in Fig. 1(b). Here we adopt the same parameters as in Refs. [34,40]: Two Ag nanospheres of radius $a = 7$ nm a nanogap $2g = 8$ nm between them centered by a QE. In work [34], where formula (2) was first derived, both these PNSs were modelled by point dipoles located at their centers. This model was validated by

comparison with [40] for the case when QE 1 is a quantum dot with d increasing from $d = 3$ D to $d = 35$ D. When $d > 5$ D the fluorescence spectrum of this system noticeably reshapes compared with the Lorentzian line. For $d = 5$–10 D the Fano resonance arises, for $d = 14$–35 D, the Rabi oscillations are seen in the simulated spectrum. The agreement of the simple dipole model [34] with the results of [40] was very good. However, fluorescence quenching at frequencies ω_+ and ω_- of Rabi oscillations was not achieved in works [34,40], where the values of d were restricted by $d \leqslant 35$ D. Frequencies ω_+ and ω_- are symmetrically distant by the Rabi frequency shift Ω from the central frequency ω_0. When we increase d [in reality, it is the same as the increase of the amount of QEs located in the nanogap of the PNA shown in Fig. 1(b)] we increase $\omega_+ - \omega_0 = \omega_0 - \omega_-$. There is no guarantee that for $d \gg 35$ D we must obtain the suppression of the fluorescence at both these frequencies.

III. STRONG COUPLING OF AN EMITTER WITH A PLASMONIC NANOSPHERE

In this section, we consider the first scenario of the strong coupling—that corresponding to Fig. 1(a) with g gradually reducing from 10 to 2 nm, whereas $a = 20$ nm. Unlike the second scenario, brings nothing physically new, and we report it as a reference case for better illustration of the claimed result. Let us discuss the approximation adopted in this model.

A fluorescent molecule is smaller than 1–1.5 nm and for the distance $g > 2$, we may consider it as a point dipole. As to PNA 2, the local field $\mathbf{E}_{12}(\mathbf{r})$ produced by QE 1 in its area (local field is calculated in absence of PNS 2) is distributed nonuniformly over this area. However, it is possible to integrate the polarization response caused by this local field numerically—either via the known Green's function of the sphere or using the commercial simulator which both allows us to find the true internal field of the sphere created by the primary dipole d_1 which is in this auxiliary study is a fixed Hertzian dipole. Integrating the internal field with corresponding weight functions we find a set of Cartesian multipoles excited in the PNS at different frequencies by a dispersion-free dipole d_1. In the range of the dipole plasmon resonance (820–850 THz) only the xx component of the quadrupole moment is noticeable (see below), though the quadrupole contribution into total polarization of the PNS is much smaller than the dipole one.

Finding the dipole moment d_2 and dividing it by $A_{12}(R)$ given by (3) we find the polarizability α_2 of the PNA for an arbitrary located effective center $x_{\text{eff}} \equiv R$ of the dipole d_2. Initially, we locate it in the geometric center of the PNS. Further, we find the local field $E_{21} = A_{12}(R)d_2$—that created by the secondary dipole d_2 at the point $x = 0$ (where dipole 1 is located) and compare it with the accurate result obtained by the integration of the elemental fields created by the elemental volumes of polarized PNS at the same point $x = 0$. This comparison has shown no practical difference for $g \geqslant 3$ nm. In other words, for the gaps larger than 2.5 nm the geometric center of the PNS can be treated as its the effective center and the impact of the quadrupole moment can be neglected. However, for $g = 2$ nm we saw a significant difference, and the change of R compared to $R = a + g$ did not reduce it. This is so because in this case the field E_{21} should comprise the quadrupole component.

A. Dipole-and-quadrupole model of the strong coupling

Local field E_{12}—that created by QE 1 at the effective center of PNS 2 in absence of the last one—is equal $E_{12} = A_{12}d_1$, where A_{12} is given by (3). Vice versa, local field E_{21}—that created by PNS 2 at the center of QE 1 in absence of the last one—is equal $E_{21} = A_{12}d_2 + B_{21}q_2$, where q_2 is the xx component of the quadrupole moment referred to the effective center of the sphere. That the effective center of PNS 2 practically does not shift from the geometric one even for $g = 2$ nm, and both dipole and quadrupole moments can be referred to the point $x_{\text{eff}} = a + g$. B_{21} is the near field of a unit quadrupole:

$$B_{21} = (3 + jkR)/8\pi\varepsilon_0\varepsilon R^4, \tag{4}$$

where $R = a + g$ as it is shown in Fig. 1(a). We calculated the quadrupole tensor whose Cartesian components $q_2^{(mn)}$ are expressed via the mth and nth components of the bulk polarization $P_{x,y,z}(\mathbf{r}') = \varepsilon_0(\varepsilon_{\text{PNS}} - \varepsilon)E_{x,y,z}(\mathbf{r})$ as follows:

$$q_2^{(mn)} = \frac{1}{2}\int_V (r'_m P_{2n} + r'_n P_{2m})\, dV. \tag{5}$$

Dipole 1 induces both dipole moment d_2 and quadrupole moment q_2 by the same local field E_{12}. Denoting the ratio of the quadrupole polarizability β_2 to the dipole polarizability α_2 as κ, we may write

$$E_{21} = A_{12}d_2 + B_{21}q_2 = A_{21}d_2, \quad A_{21} \equiv A_{12} + \kappa B_{21}. \tag{6}$$

Thus, extension of the dipole model of Refs. [34,36] to the present case yields to the seeming nonreciprocity in two interaction factors—that describing the action of QE 1 to PNS 2 and that describing the backward action. Performing the same steps as [34,36], we obtain

$$d_t = d_1^{(0)}\frac{1 + \alpha_2 A_{12}}{1 - \alpha_1\alpha_2 A_{12}A_{21}}, \tag{7}$$

$$q_2 = d_1^{(0)}\frac{\kappa\alpha_2 A_{12}}{1 - \alpha_1\alpha_2 A_{12}A_{21}}. \tag{8}$$

Formula (8) represents the self-consistent solution for the quadrupole of the sphere, and can be rewritten in a form $q_2 = \xi(R)Rd_t$, where $\xi(R)$ is a dimensionless coefficient

$$\xi(R) = \kappa\alpha_2 A_{12}/R(1 + \alpha_2 A_{12}). \tag{9}$$

Notice, however, that q_2 is not total quadrupole moment of the system which additionally to the quadrupole of the PNS comprises two dipoles with the gap R between them. Let us refer both dipole and quadrupole of the sphere to the center of the QE. Dipole moment of a particle is covariant to the origin. Quadrupole moment (Carteasin one) is not covariant and changes after this shift [41]:

$$q_2^{\text{new}} = q_2 + Rd_2 \equiv \xi(0)Rd_t, \tag{10}$$

where coefficient $\xi(0)$ relates the total quadrupole moment of the system to the total dipole moment, which in its turn is proportional to the individual dipole moment of the emitter. Really, total quadrupole moment q_t of the system is equivalent

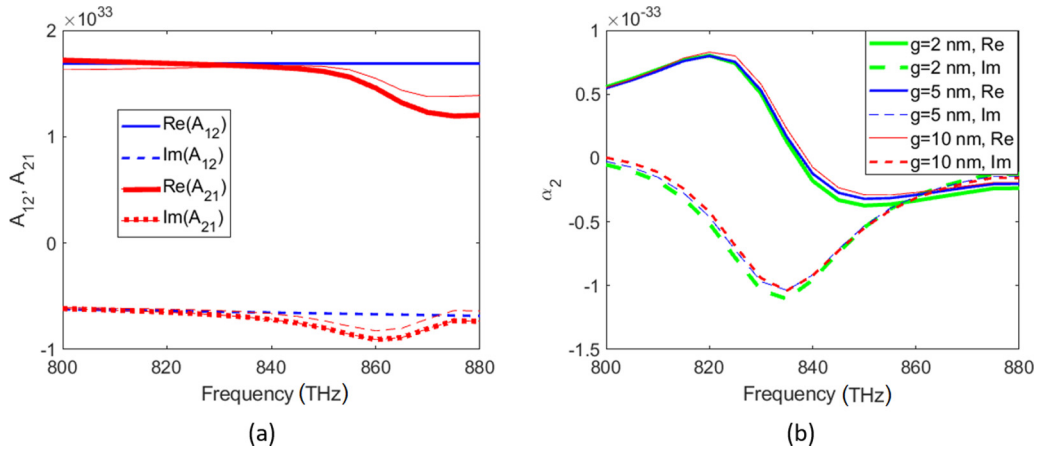

FIG. 2. (a) Frequency dependence of A_{12} and A_{21} corresponding to the choice $R = a + g$ for $g = 2$ nm. A_{12} is calculated using (3) and A_{21} is calculated either using (6) (thick red curves) or integrating the elemental dipole fields (thin red curves). (b) Dipole polarizabilities of the PNS versus frequency for different g.

to q_2^{new} because dipole $\mathbf{d}_1$ is referred to the same origin as q_2^{new} and does not contribute into it. To calculate the quadrupole moment of the system in this way is easier than to extract d_1 and d_2 from the total dipole moment d_t and calculate the quadrupole moment resulting from the gap R between these dipoles. Therefore $\xi(0)$ shows the relative contribution of the system quadrupole moment into radiation.

B. Retrieval of the model parameters

In Fig. 2(a), we show the frequency dispersion of the coupling factors A_{12} and A_{21} corresponding to the choice $R = a + g$ for $g = 2$ nm. The coincidence of A_{21} calculated using (6) with that calculated by integration of the elemental dipole fields is not exact but the relative difference between these two values is small and its mean value is minimal for $R = a + g$. It means that even for $g = 2$ nm the quadrupole moment of the PNS can be referred to its geometric center as well as the dipole moment. The action of the quadrupole is noticeable around at frequencies 850–880 THz because the resonance frequency of q_2 is equal 871 THz and the resonance band is quite broad. In Fig. 2(b), we depict the frequency dependencies of α_2 for $g = 2$, 5, and 10 nm. The case $g = 10$ nm correspond to the weak coupling (resonant F_P is nearly equal 30), whereas the case $g = 2$ nm corresponds to the strong coupling (where $F_P \ll 1$ in the whole spectrum). However, the polarizabilities of the PNS in all cases are almost the same as if the PNS was excited by a plane wave.

Then we find dimensionless quadrupole parameter $\xi(R) = \kappa/R$, corresponding to the location of the system quadrupole at the sphere center $x = R$ and the similar parameter $\xi(R)$, corresponding to the location of the system quadrupole q_2^{new} at $x = 0$. In Fig. 3, we see that at 834 THz—the frequency of the dipole resonance of the localized plasmon—parameter $\xi(0)$ exactly nullifies. It accordance to (10) it means that at the frequency of the dipole resonance the total quadrupole moment of the system vanishes. Physically it means that the quadrupole of the sphere cancels out with the quadrupole corresponding to two dipole moments d_1 and d_2 separated by the gap R.

C. Fluorescence in the case of overcritical coupling

Substituting parameters α_2, A_{12} and A_{21} into formulas (7), (10) and using (1), we calculate the frequency spectrum of the total dipole moment d_t of our system—rhodamine 123 molecule emitting at frequency 834 THz and PNS having the dipole plasmon resonance at the same frequency (parameters of Ag were taken from [38]). Next, using d_t we calculate the radiated power versus frequency using formula [41]

$$P_{\text{rad}} = \frac{\eta c^2 k^4 |d_t|^2}{12\pi}\left(1 + \frac{|q_t|^2}{120|d_t|^2}\right) = \frac{\eta c^2 k^4 |d_t|^2}{12\pi}\left(1 + \frac{|\xi(x=0)kR|^2}{120}\right), \tag{11}$$

where η is wave impedance of the ambient. Formula (11) does not contain the interference term and implies that our quadrupole and dipole are mutually coherent and refer to the same point. Using (11), we calculate also the frequency dependent radiative Purcell factor $F_P \equiv P_{\text{rad}}/P_0$ (here $P_0 = \eta c^2 k^4 |d_1^{(0)}|^2/12\pi$ is the radiation power corresponding to the

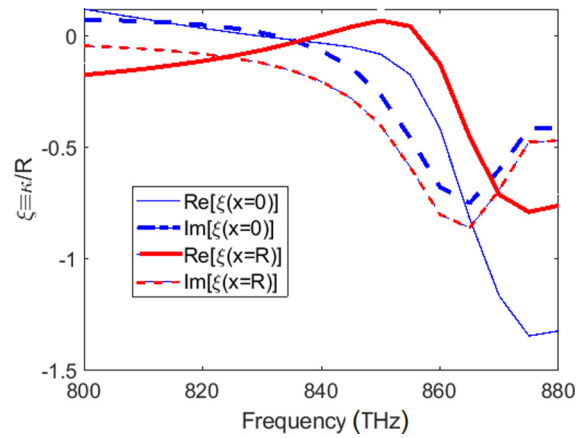

FIG. 3. Frequency dependence of the quadrupole parameter ξ for two choices of the quadrupole origin: Center of the sphere ($x = R$) and center of dipole 1 ($x = 0$).

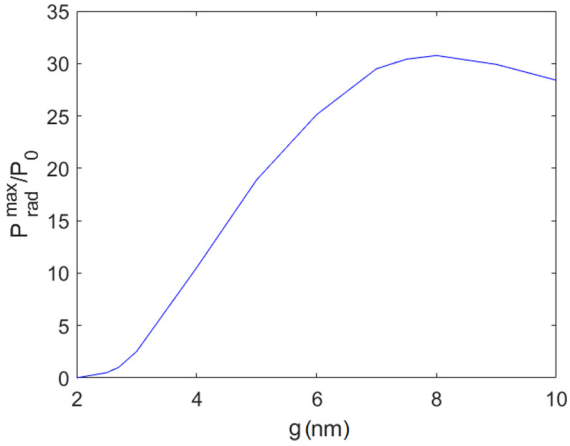

FIG. 4. Radiative Purcell factor calculated at the maximum of the spectral line as a function of the distance g between the emitter and the nanosphere.

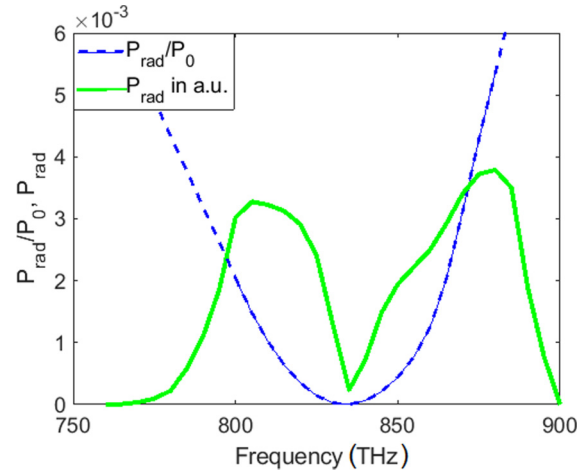

FIG. 5. Frequency dispersion of the radiated power and Purcell factor in the regime of fluorescence quenching.

single photon emission by an individual molecule of rhodamine. The gap for which the fluorescence enhancement disappears, i.e., $F_P \leqslant 1$ in the whole fluorescence spectrum is $g = 5$ nm.

When $g = 5$ nm the fluorescence spectrum is not yet reshaped, however, we already can refer this case as the strong coupling. This result is the same as that of Ref. [42], where the similar problem was solved for the same PNS using the semicalssical model [43]. The difference of the problem formulation was the coherent pumping adopted in Ref. [43] which resulted in the Mollow triplet even for a single QE. However, the bound of critical coupling when the effect of enhanced total polarization of the system turns substituted by the effect of reduced total polarization does not depend on the pumping. It is a purely linear effect and the transition from the Purcell effect to the quenching occurs smoothly. For $g < 5$ nm (this case was not calculated in Ref. [42]), the spectral line starts to reshape that can be treated as the feature of the strong coupling. In this range of g, the radiative Purcell factor decreases when the emitter approaches to the PNS.

The value $F_P^{\max}$, maximal over the spectral line, calculated as the function of g is presented in Fig. 4. The absolute maximum is achieved when the gap is equal 8 nm that corresponds to the regime of the weak coupling. For $3 < g < 5$ nm, we have $F_P(\omega_0) < 5$ whereas at the frequencies of the spectral maxima $5 < F_P(\omega_\pm) < 15$. For $g = 3$ nm, two spectral maxima which can be identified as the frequencies of Rabi oscillations $\omega_\pm = \omega_0 \pm \Omega$ arise in the emission spectrum. The regime of Rabi oscillations when $F_P^{\max}$ is still larger than unity can be referred as that of the critical coupling. The interval $2.5 < g < 3$ nm corresponds to $1 < F_P^{\max} < 5$ and $F_P(\omega_-) \approx F_P(\omega_+) \approx F_P^{\max}$. When $g = 2$–2.5 nm the fluorescence is suppressed, i.e., $F_P < 1$ in the range covering both frequencies of Rabi oscillations. This case can be referred as overcritical coupling. In this regime, dipole moments d_1 and d_2 of the emitter and the PNS compensate one another. Moreover, the quadrupole of the PNS cancels out with the quadrupole composed by two dipoles d_1 and $d_2 = -d_1$ separated by the gap $R + g$. No polarization in the system implies no radiation from it in the whole fluorescence band. The value of the gap $g = 2.5$ nm can be considered as a threshold of this regime.

In Fig. 5, we depict the radiative Purcell factor for $g = 2$ nm. Both dipole and quadrupole moments of the system practically vanish at the same frequency ω_0 [in our model $F_P(\omega_0) \approx 10^{-5}$ in this case]. The system very weakly radiates not only at ω_0, but also at both frequencies of Rabi oscillations $\omega_+ = 2\pi 882 \times 10^{12}$ rad/s and $\omega_- = 2\pi 808 \times 10^{12}$ rad/s. In our model, $F_P(\omega_+) \approx 3.9 \times 10^{-3}$ and $F_P(\omega_-) \approx 3.2 \times 10^{-3}$. The fluorescence spectrum $P_{\rm rad}(\omega)$ results from the multiplication of $P_0(\omega)$ having the maximum at ω_0 by $F_P(\omega)$ having the minimum at ω_0. The curve $P_{\rm rad}(\omega)$ is shown in Fig. 5 in arbitrary units so that to combine it with F_P on the same plot.

Two local maxima of the fluorescence we observe in Fig. 5 at frequencies $\omega_\pm$ are also the maxima of the system polarization. In our approximate model, it is not completely damped but reduced drastically. Meanwhile, inside the system the Rabi oscillations of the dipole moments d_1 and d_2 taken separately are strong. These dipoles moments have the same magnitude (which is much larger than $|d_1^{(0)}(\omega_0)|$ because the nonradiative Purcell factor at these frequencies is very high [44]) and nearly opposite phases. This is the principal difference of the Rabi oscillations in the strong coupling regime from usual normal modes of two inductively (elastically) coupled circuits (oscillators) where the higher normal mode is the opposite-phase one and the lower mode is the in-phase one.

IV. STRONG COUPLING OF AN EMITTER WITH A PLASMONIC DIMER

In the second scenario, corresponding to Fig. 1(b) the coupling increases because d of QE 1 grows. In this case ($a = 7$ nm, $g = 4$ nm), we did not need to search the effective centers of the spheres—they are definitely located at their geometric centers. Instead, we performed two CST simulations (CST meaning Computer Simulation Technology is a popular commercial electromagnetic solver) of a plasmonic dimer of spheres: (1) illuminated by a plane wave incident along y with electric field polarized along x and (2) excited by a unit Hertzian dipole centering the gap. From the first simulation,

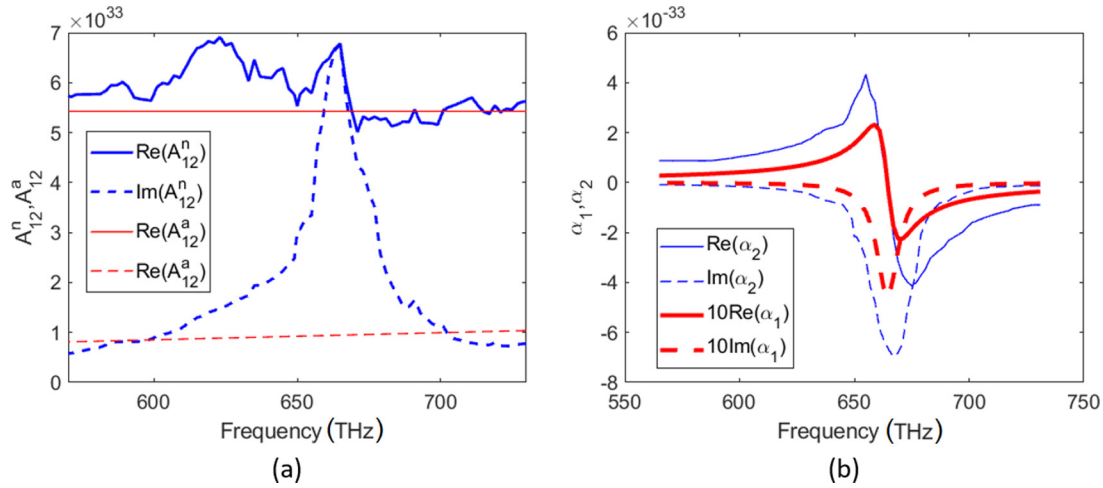

FIG. 6. (a) Frequency dependence of A^a_{12} corresponding to formula (3) and A^n_{21} corresponding to the CST simulations. (b) Dipole polarizabilities of the PNA and QE (the latter one is multiplied by 10).

we found α_2 as the ratio of d_2 (doubled dipole moment of one PNS) to the incident wave field in the plane $y = 0$. This polarizability is strongly influenced by the mutual coupling of two halves of our PNA and is different from that of a single nanosphere (much larger resonance magnitude and large red shift of the resonance). Then we found the field E_{21} produced by the PNA at the origin subtracting the incident field from the total one, and dividing this E_{21} by d_2 we found the interaction factor A_{21}. From reciprocity, we have $A_{21} = A_{12}$ because the quadrupole moment of the PNSs is negligibly small. Thus we may denote this retrieved A_{21} as A^n_{12} and call it numerical interaction factor.

From the simulation with the Hertzian dipole $d_1 = 1$, we found d_2 and using A^n_{12} calculated the polarizability of the PNA corresponding to its excitation by a Hertzian dipole $\alpha_2 = d_2/A^n_{12}$. This polarizability turned out to be equal to that corresponding to the plane-wave incidence with very high accuracy. Notice, that the point dipole model of two PNSs allows us to find A_{12} using formula (3) with $R = a + g$. This value is denoted below A^a_{12} and called analytical interaction factor.

A. Retrieval of the model parameters

In Fig. 6(a), we depict the frequency dispersion of the interaction factor A_{12}, analytically calculated using (3) and numerically simulated using the data of the plane-wave incidence problem. These values match very well except a peak of $\mathrm{Im}(A^n_{21})$ having the maximum at the plasmon resonance frequency 666 THz. However, this peak plays no important role. In Fig. 6(b), we present the polarizability of the PNA versus frequency retrieved from simulations with a Hertzian dipole using A^n_{21} extracted from simulations with a plane wave. Its real part is affected by a numerical noise, that, however, is not significant and keeps it numerically close to the real part of A^a_{21}.

If we retrieve α_2 from simulations with a Hertzian dipole using A^a_{12}, the resonant dispersion of α_2 becomes more smooth compared to that depicted in Fig. 6(a), however, the maxima of the real and imaginary parts do not change and the resonance band keeps the same. For comparison, in Fig. 6(b), we also show the polarizability of the QE for the case $d = 80$ D calculated using (1) (physically this value of d corresponds to a quantum dot whose transition dipole moment for the same fluorescence frequency ω_0 is proportional to its radius [40]). In accordance to [36], this choice of d corresponds to the slightly overcritical coupling. In this case, the condition of the strong coupling $|\alpha_1\alpha_2 A^2_{12}| > 1$ holds over the whole fluorescence spectrum of an individual QE. However, it is enough to strongly damp the radiation at the frequencies of Rabi oscillations.

B. Fluorescence at the frequencies of Rabi oscillations

Calculating the radiated power of the system, we used formula (11) taking into account the quadrupole component of the polarization corresponding to the distance $2a + 2g = 22$ nm between the dipoles of the PNA. This quadrupole radiation gives a very minor contribution, the dipole radiation dominates. This radiation is not suppressed

In Fig. 7, we depict the Purcell factor and the fluorescence spectrum (in arbitrary units) for $d = 80$ D. We can see that the dip in the frequency dependence of the Purcell factor is narrower than the interval between the frequencies of Rabi oscillations ω_+ and ω_-. The fluorescence does not quench: At $\omega_+ = 2\pi 676 \times 10^{12}$ rad/s $F_P(\omega_+) \approx 0.33$ and at $\omega_- = 2\pi 657 \times 10^{12}$ rad/s $F_P(\omega_-) \approx 0.49$. Why these values are so large, if the relative interval between the frequencies of the fluorescence ($19/666 \approx 3\%$) is triply smaller than that in the previous scenario ($74/834 \approx 9\%$)?

The dimer PNA is fivefold more narrow-band than the PNS (compare the polarizabilities in Figs. 2 and 6). Therefore, for it this Rabi splitting though lower than that in the case of a PNS corresponds to a stronger coupling. As a result, the frequencies of the fluorescence for $d = 80$ D are located near the edges of the plasmon resonance band. The fluorescence is suppressed very well [$F_P(\omega_0) \sim 10^{-7}$] in the center of the spectral range, but near the edges of the spectral band it is reduced weakly compared to that of the same quantum dot in free space. This decrease holds only in the interval

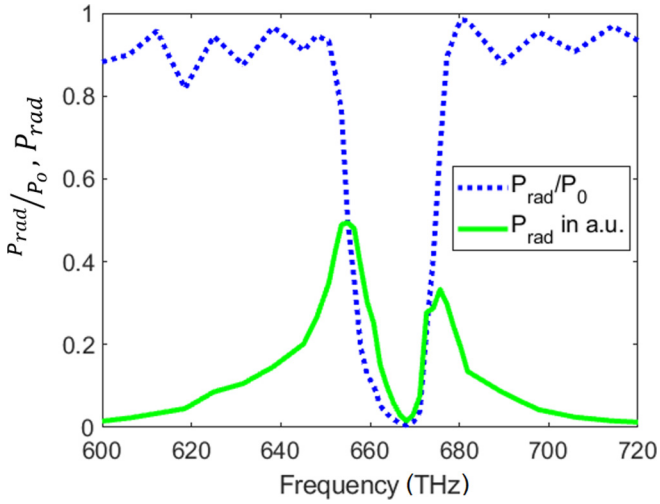

FIG. 7. Frequency dispersion of the radiated power and Purcell factor in the regime of slightly overcritical coupling.

$75 < d < 80$ D. The dependence of $F_P^{\max}$ on d—parameter determining the level of coupling—is presented in Fig. 8. It is done in the logarithmic scale because the PNA is much more efficient than a simple PNS and grants, as we can see on this figure, a very high radiative Purcell factor in the case of the optimal coupling. For $d > 80$ D the Purcell factor at the frequency ω_- starts to grow again. In other words, the PNA again enhances the fluorescence of a quantum dot, bit the enhancement occurs at a red-shifted frequency, and this frequency shift (Ω) grows versus d. For $d = 100$ D, we obtain $F_P(\omega_-) \approx 2$—the same result as for $d = 50$ D.

So, for a dimer PNA in our model, there is no overcritical coupling regime—no fluorescence quenching. A very strong coupling either slightly decreases the fluorescence or even increases it. Of course if an emitter approaches to one of two nanoparticles forming our PNA it will experience the quenching at a certain distance. However, in this geometry a cluster of many QEs is located in the dimer antenna gap symmetrically. For example, fluorescent molecules may completely fill in

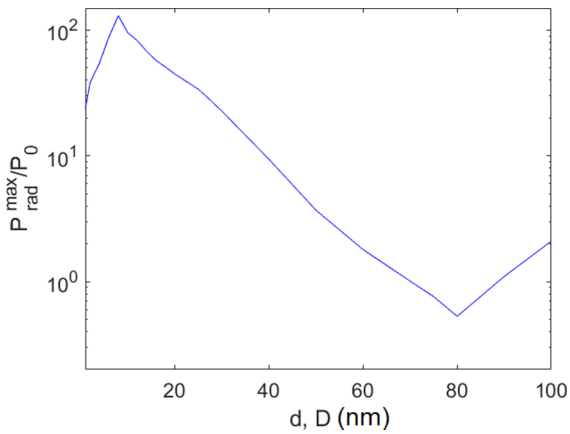

FIG. 8. Radiative Purcell factor calculated at the maximum of the spectral line as a function of the quantum dot transition dipole moment d in Debyes.

the nanogap. Fluorescence quenching of the emitting cluster centering the gap of a dimer PNA never happens (if our model is correct). Notice that the transition dipole moments as high as $d = 80$–100 D used in our numerical example, are not feasible in a single quantum dot. Above, we have considered these values conceptually, having in mind namely an array of QEs that for simplicity of the model can be replaced by a single emitter with huge d.

V. DISCUSSION AND CONCLUSIONS

If Rabi oscillations in our system keep radiative for whatever level of coupling it means that the prerequisite of the spaser is not fulfilled [15,16]. Photons are emitted to ambient instead of being fully converted into the localized plasmon, and the generation of the last one is impossible. Two questions should be discussed before we conclude this paper. Is our result reliable enough? Is it a specific property of our PNA or it should be a property of any good PNA?

Many scientists believe that the dynamic fluorescence quenching is a fundamental property of any plasmonic configuration, and it is difficult for them to accept our claims. Really, in all known studies of the strong coupling between a PNA and a QE the quenching was observed. However, as it was already mentioned, all these studies referred to poor PNAs—those which may grant the maximal value of F_P of the order of 5–20. An ultimate case of a poor PNA is a flat surface of a plasmonic metal (maximal value of F_P is 2) for which the fluorescence quenching was shown in [45]. Though a metal plane can hardly grant the spaser operation, this prerequisite of the spaser is fulfilled for it. And it is not surprising because poor PNAs are broadband. The spread of their plasmon resonance over the frequency axis is the condition of the fluorescence quenching. Only if the resonance band is broad both $\omega_- = \omega_0 - \Omega$ and $\omega_+ = \omega_0 + \Omega$ are located in this band for whatever feasible coupling. A good PNA grants not only narrowband plasmon resonance, it is narrowband as such, and the band in which it grants the resonant energy transfer regime is also narrow. This intrinsic narrow-band property means that the fluorescence cannot be suppressed at both frequencies ω_- and ω_+ whose difference is determined by the level of the coupling and is not dependent on the plasmon resonance bandwidth. For a good PNA, both these frequencies in the regime of the strong coupling are located outside the band of the localized surface plasmon and the emission turns out to be weakly coupled to the plasmon. Instead of pumping the plasmon, photons transferred to the PNA produce the enhanced system polarization and the nanolaser becomes possible.

Our result explains why a spaser can be experimentally realized with a simple nanosphere, whereas a plasmonic bowtie or a split-ring resonator granted rather efficient nanolasers. Here it worth to repeat that a nanolaser and a spaser are two very different generators of coherent oscillations. Spaser generates the near field of a localized surface plasmon. In the linear regime (precedent to the generation), its emitter experiences the nonradiative decay. Nanolaser generates the polarization which radiates also in the transition time. The excitation of a plasmon in a PNA is not necessary for it. The role of the plasmon resonance for a nanolaser is only

formation of an effective cavity resonator in the gap of the PNA [23]. The nanolaser can be implemented with an all-dielectric nanoantenna as well.

Now, about reliability of our results. Within the framework of classical electrodynamics our method is fully strict if the dipole model is generalized to a full set of electric multipoles (magnetic multipoles are not excited in the symmetric configurations of Fig. 1. For a set of multipoles, formulas (7) and (8) are continued by the similar expression for the octupole, etc., the interaction of a QE and a PNA is described exactly—this is the same as to use the Green function of the PNA. Then the difference of our model from [6,7,32] is purely positive because we take the PNA feedback into account, and these simplistic classical models do not. This generalization of our dipole-and-quadrupole model is easy. We have done it aiming to study substantially larger PNSs. However, this study brings nothing scientifically new, since PNSs with $a \gg 20$ are even more poor PNAs than the PNS with $a = 20$ nm. So, we can consider our study above as accurate enough within the framework of the classical electrodynamics.

As to the validation of the classical model by a quantum one, in Ref. [34], this has been already done. Namely for this dimer PNA our model gave basically the same results as the solution of the Maxwell-Bloch equations in Ref. [40]. The only difference is the dipole moment of the optical transition in the quantum dot that is enlarged in the present work from 35 D to 80–100 D. However, the regime under discussion is linear. The increase of the initial dipole moment of the QE can hardly disable a linear model if it is correct. Perhaps, it is worthy to additionally check our result using another quantum model—solving the Heisenberg-Langevin equations of quantum motion. However, it is not so easy for a plasmonic dimer. We hope, that the presented explanation of the effect predicted by an accurate classical model justifies the publication of this work as it is, and hope that the ideas of this paper will be useful for the future development of nanolasers and spasers.

[1] E. Dulkeith, M. Ringler, T. A. Klar, and J. Feldmann, Gold nanoparticles quench fluorescence by phase-induced radiative rate suppression, Nano Lett. **5**, 585 (2005).

[2] J. R. Lakowicz, K. Ray, M. Chowdhury, H. Szmacinski, Y. Fu, J. Zhang, and K. Nowaczyk, Plasmon-controlled florescence: A new paradigm in fluorescence spectroscopy, Analyst **133**, 1308 (2008).

[3] P. Anger, P. Bharadwaj, and L. Novotny, Enhancement and Quenching of Single-Molecule Fluorescence, Phys. Rev. Lett. **96**, 113002 (2006).

[4] T. Ribeiro, C. Baleizao, and J. P. S. Farinha, Artefact-free evaluation of metal enhanced fluorescence in silica coated gold nanoparticles, Sci. Rep. **7**, 2440 (2017).

[5] B. Valeur and M. N. Berberan-Santos, *Molecular Fluorescence: Principles and Applications*, 2d ed. (Wiley-VCH, New York, 2012).

[6] R. Carminati, J.-J. Greffet, C. Henkel, and J. M. Vigoureux, Radiative and non-radiative decay of a single molecule close ro a metallic nanoparticle, Opt. Commun. **261**, 368 (2006).

[7] *Optical Antennas*, edited by M. Agio and A. Alú (Cambridge University Press, Cambridge, UK, 2013), Chap. 3.

[8] L. Novotny and B. Hecht, *Principles of Nano-Optics* (Cambridge University Press, Cambridge, UK, 2006).

[9] S. Kühn, U. Hakanson, L. Rogobete, and V. Sandoghdar, Enhancement of Single-Molecule Fluorescence Using a Gold Nanoparticle as an Optical Nanoantenna, Phys. Rev. Lett. **97**, 017402 (2006).

[10] O. Tovmachenko, C. Graf, D. J. van den Heuvel, A. van Blaaderen, and H. C. Gerritsen, Fluorescence enhancement by metal-core/silica-shell nanoparticles, Adv. Mater. **18**, 91 (2006).

[11] F. Tam, G. P. Goodrich, B. R. Johnason, and N. J. Halas, Plasmonic enhancement of molecular fluorescence, Nano Lett. **7**, 496 (2007).

[12] H. Mertens and A. Polman, Plasmon-enhanced erbium luminescence, Appl. Phys. Lett. **89**, 211107 (2006).

[13] Q. Gu and Y. Fainman, *Purcell Effect and the Evaluation of Purcell and Spontaneous Emission Factors* (Cambridge University Press, Cambridge, UK, 2017), pp. 65–90.

[14] M. I. Stockman, Spaser Action, Loss Compensation, and Stability in Plasmonic Systems with Gain, Phys. Rev. Lett. **106**, 156802 (2011).

[15] E. S. Andrianov, A. A. Pukhov, A. V. Dorofeenko, A. P. Vinogradov, and A. A. Lisyansky, Rabi oscillations in spasers during non-radiative plasmon excitation, Phys Rev. B **85**, 035409 (2012).

[16] D. G. Baranov, E. S. Andrianov, A. P. Vinogradov, and A. A. Lisyansky, Exactly solvable toy model for surface plasmon amplification by stimulated emission of radiation, Opt. Express **21**, 10779 (2013).

[17] D. J. Bergman and M. I. Stockman, Surface Plasmon Amplification by Stimulated Emission of Radiation: Quantum Generation of Coherent Surface Plasmons in Nanosystems, Phys. Rev. Lett. **90**, 027402 (2003).

[18] M. I. Stockman, Spasers explained, Nat. Photon. **2**, 327 (2008).

[19] M. A. Noginov, G. Zhu, A. M. Belgrave, R. Bakker, V. M. Shalaev, E. E. Narimanov, S. Stout, E. Herz, T. Suteewong, and U. Wiesner, Demonstration of a spaser-based nanolaser, Nature (London) **460**, 1110 (2009).

[20] P. Song, J.-H. Wang, M. Zhang, F. Yang, H.-J. Lu, B. Kang, J.-J. Xu, and H.-Y. Chen, Three-level spaser for next-generation luminescent nanoprobe, Sci. Adv. **4**, eaat0292 (2018).

[21] S. Maslovski and C. Simovski, Purcell factor and local intensity enhancement in surface-enhanced Raman scattering, Nanophotonics **8**, 429 (2019).

[22] S. W. Chang, C. Y. A. Ni, and S. L. Chuang, Theory for bowtie plasmonic nanolasers, Opt. Express **16**, 10580 (2008).

[23] I. E. Protsenko, A. V. Uskov, O. A. Zaimidoroga, V. N. Samoilov, and E. P. O'Reilly, Dipole nanolaser, Phys Rev. A **71**, 063812 (2005).

[24] A. S. Rosenthal and T. Ghannam, Dipole nanolasers: A study of their quantum properties, Phys. Rev. A **79**, 043824 (2009).

[25] M. T. Hill, Y. S. Oei, B. Smalbrugge, Y. Zhu, T. de Vries, P. J. van Veldhoven, F. W. M. van Otten, T. J. Eijkemans, J. P. Turkiewicz, H. de Waardt, E. J. Geluk, S. H. Kwon, Y. H. Lee, R. Notzel, and M. K. Smith, Lasing in metallic-coated nanocavities, Nat. Photonics **1**, 589 (2007).

[26] J. Y. Suh, C. H. Kim, W. Zhou, M. D. Huntington, D. T. Co, M. R. Wasielewski, and T. W. Odom, Plasmonic bowtie nanolaser arrays, Nano Lett. **12**, 5769 (2012).

[27] N. I. Zheludev, S. L. Prosvirnin, N. Papasimakis, and V. A. Fedotov, Lasing spaser, Nat. Photonics **2**, 351 (2008).

[28] P. Melentiev, A. Kalmykov, A. Gritchenko, A. Afanasiev, V. Balykin, A. S. Baburin, E. Ryzhova, I. Filippov, I. A. Rodionov, I. A. Nechepurenko, A. V. Dorofeenko, I. Ryzhikov, A. P. Vinogradov, A. A. Zyablovsky, E. S. Andrianov, and A. A. Lisyansky, Plasmonic nanolaser for intracavity spectroscopy and sensorics, Appl. Phys. Lett. **111**, 213104 (2017).

[29] T. Yoshie, O. B. Shchekin, H. Chen, D. G. Deppe, and A. Scherer, Quantum dot photonic crystal lasers, Electron Lett. **38**, 967 (2002).

[30] D. L. Andrews and D. S. Bradshaw, Virtual photons, dipole fields and energy transfer: A quantum electrodynamical approach, Eur. J. Phys. **25**, 845 (2004).

[31] J. R. Lakowicz, *Principles of Fluorescence Spectroscopy*, 2d ed. (Kluwer Academic, NY, 1999), pp. 374–443.

[32] T. Förster, Zwischenmolekulare Energiewanderung und Fluoreszenz, Ann. Phys. **437**, 55 (1948).

[33] A. Kurs, A. Karalis, R. Moffatt, J. D. Joannopoulos, P. Fisher, and M. Soljacic, Wireless power transfer via strongly coupled magnetic resonances, Science **317**, 83 (2007).

[34] C. Simovski, Circuit model of plasmon-enhanced fluorescence, Photonics **2**, 568 (2015).

[35] A. E. Krasnok, A. P. Slobozhanyuk, C. R. Simovski, S. A. Tretyakov, A. N. Poddubny, A. E. Miroshnichenko, Y. S. Kivshar, and P. A. Belov, An antenna model for the Purcell effect, Sci. Rep. **5**, 12956 (2015).

[36] C. Simovski, Point dipole model for metal-enhanced fluorescence, Opt. Lett. **44**, 2697 (2019).

[37] P.-H. Chung, C. Tregidgo, and K. Suhling, Determining a fluorophore's transition dipole moment from fluorescence lifetime measurements in solvents of varying refractive index, Methods Appl. Fluoresc. **4**, 045001 (2016).

[38] E. D. Palik, *Handbook of Optical Constants* (Academic Press, NY, 1985).

[39] *Gold Nanoparticles For Physics, Chemistry And Biology*, 2nd ed., edited by C. Louis and O. Pluchery (World Scientific Publishing Europe, London, 2017), p. 404.

[40] S. Savasta, R. Saija, A. Ridolfo, O. Di Stefano, P. Denti, and F. Borghese, Nanopolaritons: Vacuum Rabi splitting with a single quantum dot in the center of a dimer nanoantenna, ACS Nano **4**, 6369 (2010).

[41] R. E. Raab and O. L. de Lange, *Multipole Theory in Electromagnetism* (Oxford University Press, Oxford, UK, 2005).

[42] Y. V. Vladimirova, V. V. Klimov, V. M. Pastukhov, and V. N. Zadkov, Modification of two-level-atom resonance fluorescence near a plasmonic nanostructure, Phys. Rev. A **85**, 053408 (2012).

[43] H. J. Kimble and L. Mande, Theory of resonant fluorescence, Phys. Rev. A **13**, 2123 (1976).

[44] C. Simovski, Circuit theory of metal-enhanced fluorescence, Phot. Nanostruct. Fund. Appl. **36**, 100712 (2019).

[45] I. A. Larkin, M. I. Stockman, M. Achermann, and V. I. Klimov, Dipolar emitters at nanoscale proximity of metal surfaces: Giant enhancement of relaxation n microscopic theory, Phys. Rev. B **69**, 121403 (2004).